Theor Chem Acc (2011) 130:1169–1183
DOI 10.1007/s00214-011-1054-1

REGULAR ARTICLE

Ground-state properties of the retinal molecule: from quantum mechanical to classical mechanical computations of retinal proteins

Ana-Nicoleta Bondar · Michaela Knapp-Mohammady · Sándor Suhai · Stefan Fischer · Jeremy C. Smith

Received: 8 July 2011 / Accepted: 19 September 2011 / Published online: 29 October 2011

Abstract Retinal proteins are excellent systems for understanding essential physiological processes such as signal transduction and ion pumping. Although the conjugated polyene system of the retinal chromophore is best described with quantum mechanics, simulations of the long-timescale dynamics of a retinal protein in its physiological, flexible, lipid-membrane environment can only be performed at the classical mechanical level. Torsional energy barriers are a critical ingredient of the classical force-field parameters. Here we review briefly current retinal force fields and discuss new quantum mechanical computations to assess how the retinal Schiff base model and the approach used to derive the force-field parameters may influence the torsional potentials.

Keywords Retinal · Retinal proteins · Quantum mechanical · Force-field parameters

Dedicated to Professor Akira Imamura on the occasion of his 77th birthday and published as part of the Imamura Festschrift Issue.

Present Address:
A.-N. Bondar (✉)
Theoretical Molecular Biophysics, Department of Physics, Freie Universität Berlin, Arnimallee 14, 14195 Berlin, Germany
e-mail: nbondar@zedat.fu-berlin.de

A.-N. Bondar
Department of Physiology and Biophysics, School of Medicine, University of California at Irvine, Med. Sci. I, D374, Irvine, CA 92697-4560, USA

M. Knapp-Mohammady
Molecular Biophysics Department and Division of Functional Genome Analysis, German Cancer Research Center, Im Neuenheimer Feld 580, 69120 Heidelberg, Germany

S. Suhai
Molecular Biophysics Department, German Cancer Research Center, Im Neuenheimer Feld 580, 69120 Heidelberg, Germany

1 Introduction

Retinal proteins are seven-helical membrane proteins in which the retinal chromophore is covalently bound to a Lys amino acid residue via a protonated Schiff base (for reviews see, for example, Refs. [1–4]). The large family of retinal proteins includes light receptors such as the visual rhodopsin G-protein-coupled receptors (GPCRs), chloride and proton pumps. In these proteins, absorption of light by the retinal chromophore triggers a reaction cycle that involves changes in the retinal isomeric state, changes in protein conformation, and proton transfer. The ability of retinal proteins to transport ions in response to light absorption and retinal photoisomerization is being exploited in biotechnology and neurobiology applications. For example, the proton pumping bacteriorhododopsin from *Halobacterium salinarium* could be used in data-storing devices [5], and the cation channel channelrhodopsin-2 and

S. Fischer
Computational Biochemistry, IWR, University of Heidelberg, Speyerstrasse 6, room H304, 69115 Heidelberg, Germany

J. C. Smith (✉)
Oak Ridge National Laboratory, PO Box 2008 MS6164, Oak Ridge, TN 37831-6164, USA
e-mail: smithjc@ornl.gov

J. C. Smith
Department of Biochemistry and Molecular Biology, University of Tennessee, M407 Walters Life Sciences, 1414 Cumberland Ave, Knoxville, TN 37996, USA

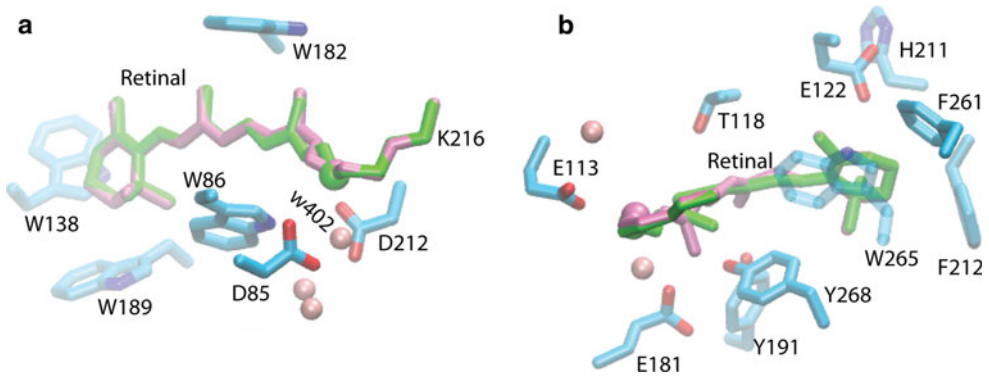

Fig. 1 Retinal geometry in the complex environment of the opsin proteins. **a** The all-*trans* (*green*) and 13-*cis* retinal (*purple*) in the bacteriorhodopsin ground- and K-state intermediate, respectively. The Schiff base nitrogen is indicated by a small sphere. Selected protein amino acids and water molecules in the ground state are also depicted, with water molecules shown as *pink spheres*. Note the twisted geometry of the retinal, and the acidic amino acids and the water molecules close to the retinal Schiff base; Trp amino acids are located close to the retinal polyene chain and to the β-ionone ring. **b** The 11-*cis* (*green*) and all-*trans* retinal (*purple*) in the bovine rhodopsin dark- and batho-states, respectively, with the Schiff base indicated by a *small spheres*. Selected protein amino acids and water molecules in the *dark state* are depicted explicitly. Note the highly twisted geometry of the retinal in the both dark- and batho-states, the close packing of protein amino acids close to the retinal molecule, and the presence of charged/polar amino acids close to the retinal. Figure 1 was prepared using the VMD software [104] based on the crystal structures of [29, 67, 105, 106]

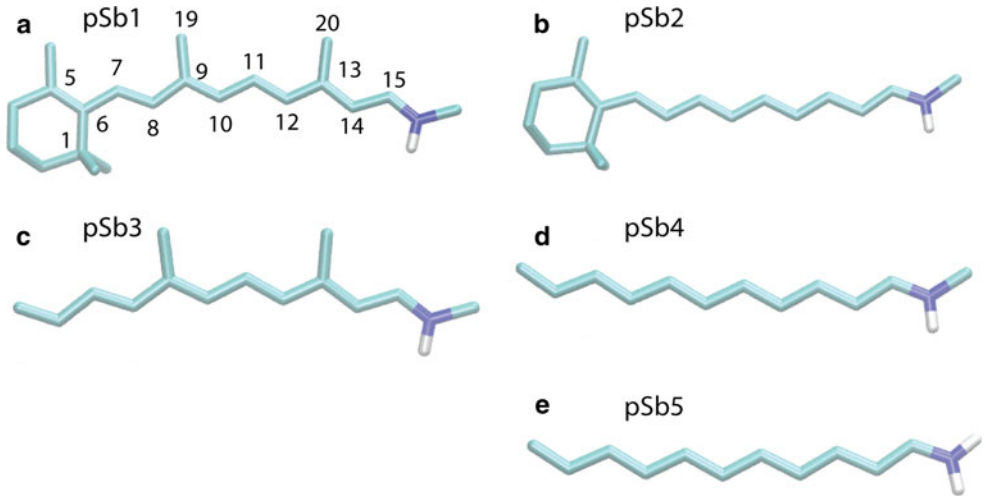

Fig. 2 Schematic representation of the retinal models used. **a**–**e** Depict the five retinal protonated Schiff base models pSb1–pSb5 (B3LYP/6-31G* optimized geometries). For simplicity, only the hydrogen atom(s) covalently bound to the Schiff base nitrogen is/are shown explicitly. The *numbers* in **a** indicate the numbering of the carbon atoms. Note the subtle effects that the methyl groups on C_9 and C_{13} have on the overall shape of the retinal molecule (compare **a** with **b**, and **c** with **d**). The molecular graphics images from Figs. 2, 3, 6 and 8 were prepared with the VMD software [104]

the chloride pump halorhodopsin are used in optogenetics applications (see, e.g., Refs. [6–9]).

Understanding and manipulating the functioning of retinal proteins benefit greatly from computer simulations. A difficulty that arises in theoretical studies of retinal proteins is the need to describe accurately the conjugated polyene system of the retinal molecule, which is best treated with appropriate quantum mechanical (QM) methods; indeed, numerous high-level QM computations have been performed to assess the physical–chemical properties of retinal Schiff base models (e.g., Refs. [10–15]). Interactions with the protein environment (see Fig. 1 for an illustration of the binding pockets of the retinal in bacteriorhodopsin and bovine rhodopsin) can affect significantly the physical–chemical properties of the retinal. Importantly, hydrogen-bonding to water stabilizes the protonated state of the retinal Schiff base [16] and can affect the conformation of the retinal in the protein environment [17, 18]; interactions with the tight binding pocket of the visual bovine rhodopsin affect the geometry of the retinal [19], the calculated proton affinity of the retinal depends on the dielectric constant used to model environmental effects [20], and electrostatic

interactions with negatively charged ions can influence the torsional barrier for the retinal C_{13}=C_{14} bond [21] (see Fig. 2a for numbering of the retinal atoms). The importance of the charged groups of the protein for the potential energy surface of the chromophore was demonstrated in the pioneering work from Refs. [22–25]. It was demonstrated, for example, that allowing the bond lengths to vary during isomerization and accounting for the effect of the external charges can modify significantly the ground-state potential for retinal double-bond torsion [23].

The quantum mechanical/molecular mechanical (QM/MM) approaches combine the QM treatment of the reaction region (typically, $\sim$100 atoms) with the MM description of the protein environment [26–28]. QM/MM studies have provided valuable information on important aspects of retinal protein function, such as the geometry of the twisted retinal in the bovine rhodopsin crystal structure [29], the role of hydrogen-bonding in storing the energy of the absorbed photon [30, 31], and the likely protonation state of an aspartate residue that may be critical for signal transduction in the visual squid rhodopsin [32].

Due to computational costs, QM/MM approaches are limited with respect to the timescale of the dynamics that can be sampled efficiently—typically, in the order of picoseconds to nanoseconds. There are key aspects of retinal protein function—for example, conformational changes and the role of water molecules in propagating conformational change [33], or how lipid molecules influence the functioning of visual rhodopsin [34]—that require prolonged ($\sim$100 ns) sampling of the protein dynamics in the explicit, hydrated lipid-membrane environment. At the moment, such simulations can only be performed with a classical MM description.

Treatment of the retinal molecule with MM requires a set of force-field parameters that, together with the potential energy function, allow us to relate the structure of the protein to its conformation and energy. The accuracy of the force-field parameters used for the retinal is essential for the reliability of the computations, and changes in the parameters can affect the results qualitatively. For example, computations with different force constants for the C_{13}=C_{14} and C_{15}=N dihedral angle torsions indicated that the nature of the all-*trans* to 13-*cis*, 15-*syn* retinal isomerization path depends on the choice of force constants [17] (see Fig. 2a for the numbering of the retinal atoms). Small changes in the MM partial charges of the retinal Schiff base affect the energy of interaction between the Schiff base and water [35]; the accurate description of the Schiff base–water interaction is essential, because hydrogen-bonding to water affects the preferred configuration of the retinal [17, 18].

Recent work on squid rhodopsin has again highlighted how important the retinal parameters are for MM computations of retinal proteins: due to the strong coupling between the retinal, protein, and water in squid rhodopsin, the use of different sets of parameters not only led to noticeable differences in the retinal geometry, but also affected the local protein structure and the dynamics of internal water molecules [36].

Here we review briefly the ground-state properties of the retinal molecule and several different sets of MM parameters that are being used to describe retinal and discuss new QM computations that help assess and compare different MM computations on retinal proteins.

1.1 The ground-state properties of the retinal as described by QM

Critical issues in describing the retinal molecule are the retinal bond alternation, the torsional properties, and the interactions between retinal, water, and charged protein amino acids.

It is a challenge for the electronic structure methods to describe the ground-state properties of the highly correlated π-electron system of the retinal polyene chain. Importantly, the geometrical parameters of the retinal polyene chain may depend upon the QM method used to derive them. Below we discuss how QM methods that have been employed to derive retinal parameters perform in describing the retinal bond alternation, torsional properties, and interaction with water.

Hartree–Fock (HF) methods, which lack dynamic correlation, indicate a large bond alternation of the single and double bonds of the retinal polyene chain. At the HF/6-31G** level, the bond alternation of all-*trans* retinal [37] is in excellent agreement with the crystal structure of isolated retinal (vitamin-A aldehyde) [38]. For example, the lengths of the C_{14}–C_{15}, C_{13}=C_{14}, and C_{12}–C_{13} retinal bonds are, respectively, 1.455, 1.344, and 1.452 Å in experiment [38], and 1.470, 1.338, and 1.471 Å with HF/6-31G** [37]. Density Functional Theory in the Generalized Gradient Approximation (DFT-GGA) methods overestimate significantly the polarizability of extended conjugate systems [39], leading to an underestimation of the bond alternation of the retinal polyene chain. DFT calculations on retinylidene iminium salts indicated that DFT reproduces the reduction in retinal bond alternation upon protonation [40]. MP2, CASPT2, and B3LYP tests on the all-*trans* penta-3,4 dieneiminium cation (with 6-31G*) [41] and MP2 and B3LYP tests on the full retinal molecule using 6-31G** [42] indicated very similar distributions of the polyene chain bond lengths, although the length of the C_{13}=C_{14} bond is slightly longer with DFT than with MP2 [42]. The underestimated bond alternation with B3LYP is also illustrated by tests on a protonated Schiff base model with four double bonds; for that model, the bond lengths for C_{12}–C_{13}, C_{13}=C_{14}, and C_{14}–C_{15} are 1.412, 1.385, and

1.398 Å, with B3LYP, and 1.439, 1.362, and 1.423 Å with CAS-SCF (8,8) (6-31G* basis set; [43]). Indeed, it had been noted that the retinal bond alternation calculated with DFT methods, including B3LYP, may be too low in comparison with the experimental data [29, 40, 44].

The torsional barrier is defined as the difference between the energy of the 90°-twisted geometry and the energy of the all-*trans* retinal. Rotation around a nominal double bond of retinal's conjugated polyene system is a particular case of chemical bond breaking, and high-level QM methods may be necessary to describe correctly the bi-radical character of the transition state [43]. The careful analysis discussed in Refs. [12, 43] demonstrates that although B3LYP has limitations inherent to DFT methods in describing the bond alternation, it provides a balanced description of the retinal ground-state properties. Importantly, it was found that B3LYP is triplet stable at the planar geometry [43] and that it is reliable for computing torsional barriers. For the protonated Schiff base model with six double bonds, the torsional barriers for the single bonds are the same when computed with B3LYP/6-31G* and UB3LYP/6-31G*; B3LYP also gives the same values with UB3LYP for the double-bond torsions close to the protonated Schiff base (C_{15}=N, C_{13}=C_{14}, and C_{11}=C_{12}), albeit overestimating the torsional barriers of the C_9=C_{10} and C_7=C_8 bonds by 3.7 and 9.2 kcal/mol, respectively [12]. Due to the overestimation of the bond alternation in DFT calculations, the barriers for rotating around the double bonds are lower with B3LYP than with CAS-SCF; for a protonated Schiff base model with four double bonds, the barrier for the C_{13}=C_{14} torsion is 39.0 kcal/mol with B3LYP, and 43.2 kcal/mol with CAS-SCF (8,8) (6-31G* basis set, see Ref. [43]); for the single bonds, B3LYP overestimates the torsional barriers. Vibrational frequency computations further verified the use of B3LYP/6-31G* for describing protonated Schiff bases [43]. In the case of the unprotonated retinal Schiff base model, however, only the single-bond torsions can be treated reliably with closed-shell calculations; double-bond isomerizations of the unprotonated species need to be described with open-shell calculations [12].

Crystal structures of retinal proteins indicate that water molecules may be found within hydrogen-bonding distances from the protonated retinal Schiff base (Fig. 1). A careful QM examination of the interactions between retinal Schiff base models and water led to the observation that accounting for electron correlation may affect the values computed for the energy of the hydrogen-bonding interactions between retinal and water molecules [45].

1.2 Force-field parameters for the retinal molecule

Several MM force fields exist for describing protein amino acids and related compounds (e.g., CHARMM [46], Amber [47], OPLS [48], GROMOS [49], CFF93 [50]). In what follows, we discuss the main features and applicability of force-field parameters used to describe the retinal molecule.

A very reliable force field for describing the retinal molecule and its physical–chemical properties is the QCFF/PI (quantum mechanical extension of the consistent force field method to PI electron molecules) [51, 52]. An important feature of QCFF/PI is that it includes the computation of π electron surfaces of conjugated molecules using a semi-empirical SCF-MO-CI procedure (Self-Consistent Field Molecular Orbital Configuration Interaction). QCFF/PI has been used, for example, to first capture the dynamics of the protonated retinal Schiff base for describing the molecular events during retinal photoisomerization in rhodopsin [52], to simulate the dynamics of the retinal photoisomerization in bacteriorhodopsin and explore the nature of the surface crossing process [53, 54], or to assess the coupling between charge stabilization, bond twist, and bond alternation [23]. Recently, the combination of QCFF/PI with the empirical valence bond method (EVB; [28]) was used to analyze the energetics of the charge separation between the positively charged retinal Schiff base and the negatively charged Asp85 counterion [55] (see also Fig. 1b).

To illustrate how the interactions between the atoms of the systems are computed within a MM approach, we use here the potential energy function of CHARMM [46], which was used extensively to study retinal proteins using classical mechanical approaches (e.g., [18, 36, 56–59]). The potential energy function of CHARMM is the sum of bonded and non-bonded interactions. The bonded interactions consist of bond stretching, bond angle bending, dihedral and improper angle contributions, and Urey-Bradley 1:3 interactions. The non-bonded interactions consist of Coulombic and van der Waals interactions. The full function is as follows:

$$
\begin{aligned}
V(r) = & \sum_{\text{bonds}} K_b(b-b_0)^2 + \sum_{\text{angles}} K_\theta(\theta-\theta_0)^2 \\
& + \sum_{\text{dihedrals}} K_\chi(1+\cos(n\chi-\delta)) \\
& + \sum_{\text{Urey-Bradley}} K_{UB}(S-S_0)^2 + \sum_{\text{impropers}} K_\phi(\phi-\phi_0)^2 \\
& + \sum_{i,j}\left(\varepsilon_{ij}\left[\left(\frac{R_{\min,ij}}{r_{ij}}\right)^2 - \left(\frac{R_{\min,ij}}{r_{ij}}\right)^6\right] + \frac{q_i q_j}{\varepsilon_D r_{ij}}\right)
\end{aligned}
$$

where b, u, θ, ϕ, δ, and ω are bond lengths, Urey–Bradley 1:3 distances, valence angles, dihedrals, phase angles, and improper angles, respectively; b_0, θ_0, and ω_0 are reference values, n is the multiplicity, and δ the phase. K_b, K_θ, K_χ, K_{UB}, and K_ω are force constants for bond stretching, angle bending, Urey Bradley 1:3 interactions, dihedral angle torsions, and out-of-plane deformations, respectively. R_{ij} and ε_{ij} describe the Lenard–Jones interactions between

atoms i and j separated by the distance r_{ij}, with ε the Lenard–Jones depth and $R_{\min}$ the distance at the minimum value of the Lenard–Jones interaction energy. q_i and ε_D give the partial atomic charge of atom i and the dielectric constant, respectively. Polarization effects can be included implicitly by optimizing the partial charges to reproduce the QM interaction energies between the model compound and water or model compound dimers, and by using HF/6-31G* to calculate the atomic partial charges [60]. We also note that the CHARMM potential energy function for protein amino acids has been recently improved by including ϕ, ψ cross-terms and dihedral energy grid correction map (CMAP) [61].

Nina et al. [35] used gas-phase HF/6-31G* computations of protonated retinal Schiff base models to derive retinal bond lengths, valence bond angles, and partial charges. The partial charges of the retinal atoms were derived from Mulliken population analysis of retinal Schiff base model/water complexes. Two different locations of the water molecule were considered one in which the water molecule hydrogen bonds to the retinal Schiff base and the other in which the water molecule hydrogen bonds to the $C_{15}H$ group. The charge and van der Waals parameters were adjusted so as to reproduce the ab initio geometries and/or the Schiff base–water interaction energies [35, 62]. The torsional potential for the C_{14}–C_{15} bond was computed with HF/6-31G* [35], and HF/6-31G* torsional barriers computed for butadiene [63] were used for the other single C–C bonds. The C=C torsional barriers were taken from valence bond computations [64]; torsional parameters for rotations around the C_{13}=C_{14} and C_{15}=N bonds were further refined so as to reproduce the HF/6-31G* results on N-methyl-methyl-3-pentenylidenimine [62]. MM simulations using the retinal parameters from Nina et al. [35, 62, 63] reproduced to within $\sim k_BT$ the experimental value for the free energy difference between the 13-*cis*, 15-*syn* and the all-*trans* retinal conformers [17] and predicted high probabilities for the presence of water molecule w402 of bacteriorhodopsin [57, 65], as was indeed revealed by high-resolution crystal structures (Fig. 1a; [66, 67]).

The force field used by Tajkhorshid et al. [56] is based on a detailed set of gas-phase B3LYP/6-31G* computations and Mulliken population analysis [12]. The B3LYP/6-31G* torsional barriers for the bonds in the Schiff base segment are significantly higher than those of the HF-derived values from Refs. [35, 63]. For example, the B3LYP/6-31G* torsional potential of the C_{14}–C_{15} bond is described by a single two-fold torsional term with a force constant of 30.4 kcal/mol [12, 56]. In the force field of Nina et al. [17, 45, 63], the torsional potential for the same bond is described by 1, 2, 3, and fourfold dihedral terms with force constants ranging from 0.4 (the fourfold term) to 5.3 kcal/mol (the twofold term). The parameter set based on the computations from Ref. [56] allowed a reliable description of the geometry of the retinal in bacteriorhodopsin [56] and was used together with that from Ref. [62] in the first molecular dynamics (MD) study of bacteriorhodopsin in the purple membrane [57]. The bonded parameters from Ref. [56] together with retinal partial charges derived from QM/MM MD simulations [68] were used to describe the retinal *cis–trans* isomerization in bovine rhodopsin [69]. Gruia et al. [70] used a hybrid retinal force field based on Ref. [35], but with the bond torsional terms adjusted to reproduce the B3LYP values from Ref. [56].

The two retinal parameter sets discussed above were derived based on gas-phase QM computations on retinal Schiff base models [17, 35, 56, 63], or on Schiff base models interacting with water [35]. In contrast, Lemaître et al. [71] derived a parameter set to reproduce the QM geometry of 11-*cis* retinal in the bovine rhodopsin-binding pocket as proposed in Ref. [19]. The partial charges on the retinal molecule were set to zero except for the nitrogen atom, the hydrogen bound to the nitrogen, C_{15}, and Cε; for these atoms, Mulliken DFT charges were used [71]. The Self-Consistent Charge Density Functional Tight Binding (SCC-DFTB, [72]) computations from Ref. [19] led to a geometry of the retinal molecule that is in very good agreement with NMR experiments [73]. Lemaitre et al. [71] used for the torsional barriers in the C_{12}–N_{16} Schiff base segment values $\sim$3–5 kcal/mol lower than those from Refs. [12, 69]. The MD simulations [71] indicated a flexible and twisted retinal in the 11-*cis* dark state of bovine rhodopsin, and a batho all-*trans* model compatible with observations from NMR.

2 Methods

2.1 Protonated retinal Schiff base models

To assess how the retinal Schiff base model used to derive the parameters influences the values of the parameters, we performed computations on five different retinal protonated Schiff base models (pSb1–pSb5, Fig. 2) that are distinguished by the substitutions along the retinal polyene chain. In pSb1–pSb4 (Fig. 2a–d), the lysine side chain to which retinal binds in the protein is modeled by a methyl group, whereas in pSb5 the lysine side chain is modeled by a H atom (Fig. 2e). pSb1 is the complete retinal molecule containing the β-ionone ring and methyl groups on C_9 and C_{13} (Fig. 2a). In pSb2 (Fig. 2b), the C_9 and C_{13} methyl groups were replaced by H atoms. pSb3 (Fig. 2c) contains the C_9 and C_{13} methyl groups, but the β-ionone ring is absent, C_1 and C_5 being replaced by H atoms. pSb4 (Fig. 2d) contains neither the C_9 and C_{13} methyl groups, nor the β-ionone ring; in pSb5 (Fig. 2e) we further simplified pSb4 by replacing with H the methyl group bound to

the nitrogen atom. pSb5 has the same chemical structure as the retinal model used for deriving the B3LYP/6-31G* torsional barriers in Ref. [12].

2.2 QM geometry optimizations and calculations of torsional energy barriers

To investigate how the constraints used to set a dihedral angle value influence the torsional energy barriers, we performed four sets of computations as described below.

In three sets of computations, we used the Gaussian software [74] to optimize the geometry at the B3LYP/6-31G* level; to generate the 90°-twisted geometries, in each set of the computations we used one of the following constraints: C-I is a single constraint applied on heavy atoms of the retinal polyene chain (Fig. 3a); C-II is a triple constraint consisting of C-I plus two additional constraints that involve the hydrogen atom or the methyl groups covalently bound to the carbon atoms of the bond being twisted (Fig. 3b); C-III is a single constraint that involves the hydrogen atom or the methyl groups covalently bound to the carbon atoms of the bond being twisted, and the carbon atoms adjacent to those of the twisted bond (Fig. 3c).

In the fourth set of computations on how the constraint affects the torsional barriers, we optimized minimum-energy paths for retinal isomerization using the Conjugate Peak Refinement (CPR) [75] as implemented in the TreK module of CHARMM [46]. The CPR calculations were performed using SCC-DFTB [72] as implemented in CHARMM [76]. We have described in detail the application of CPR to QM/MM calculations on bacteriorhodopsin [77]. Briefly, CPR is an algorithm for finding the minimum-energy paths connecting the two end states of the reaction (in our case, the all-*trans* and the *cis* retinals). In the absence of an initial guess of the path, CPR starts with a straight-line interpolation between the end states; the calculation then proceeds by either adding or removing a path segment during each iteration of the procedure. For example, in the first iteration, the segment is identified that has the highest energy along the initial guess of the path. The highest energy structure along the high-energy segment is energy-maximized along the one-dimensional vector tangent to the peak segment; the energy-maximized structure is then geometry-optimized by performing line minimizations along the directions conjugate to the peak segment, and the path segment is removed if a maximum cannot be found locally. If intermediate path points are provided the initial path, they are optimized along with the other path points. A CPR computation is completed when all energy maxima along the path are first-order saddle points. The CPR path was further refined using the Synchronous Chain Minimization algorithm (SCM) [78], which optimizes the path segments between the stationary

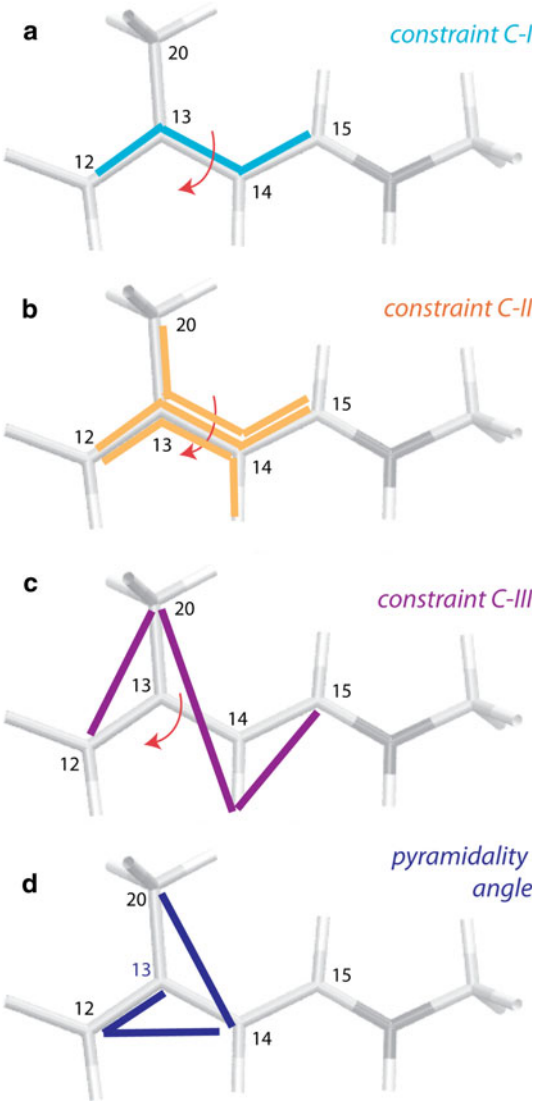

Fig. 3 Definitions of the constraints used to drive the torsions around the retinal bonds and for measuring the pyramidality. All dihedral definitions are illustrated here for the C_{13}=C_{14} twist. The *red arrow* in **a**–**c** indicates the bond being twisted. **a** Constraint C-I is a single-dihedral constraint applied on carbon atoms of the retinal polyene chain. **b** Constraint C-II is a triple constraint that maintains at 90° not only the dihedral angle defined by the carbon atoms of the polyene chain, but also two dihedral angles involving the hydrogen atom or the methyl group bound to each of the two carbon atoms that form the bond being twisted. **c** Constraint C-III is a single-dihedral constraint that involves the carbon atoms adjacent to those forming the twisted bond, and the hydrogen atom or methyl group bound to the carbon atoms of the bond being twisted. **d** Illustration of the dihedral angle used to evaluate the pyramidality at the C_{13} atom

points. The SCM-optimized isomerization path was then subject to an additional cycle of CPR computation.

To avoid highly unfavorable geometries that would be generated by CPR as a first-guess straight-line interpolation between the all-*trans* and *cis* retinal states, we introduced in the initial path intermediate path points generated using the coordinate driving protocol; the coordinate driving

intermediate path points were obtained by slowly driving the dihedral angle from its value in the all-*trans* isomer to that in the *cis*-isomer in steps of 10° and energy optimizing, for each value of the reaction coordinate, with respect to all remaining degrees of freedom.

To assess the performance of recent DFT functionals in describing the retinal molecule, we performed a set of computations on the torsional barriers of the C_{12}–C_{13}, C_{13}=C_{14}, C_{14}–C_{15}, and C_{15}=N bonds using the following recent hybrid DFT functionals: CAM-B3LYP (Coulomb-attenuating method B3LYP, [79]), which is the long-range corrected version of B3LYP; B3PW91 [80–84]; BMK (Boese–Martin for kinetics; [85]), which has been optimized to describe barrier heights; LC-wPBE (long-range corrected wPBE, [86]); M05-2X [87] and M06-2X [88]. All test calculations using these recent DFT functionals were performed with Gaussian09 [89] using model pSb1 (Fig. 2a), constraint C-I, and the 6-31G* basis set.

3 Results

The detailed computations performed here demonstrate the significant dependence of specific retinal torsional barriers on the retinal Schiff base model employed for the computations. Furthermore, we find noticeable differences in the retinal torsional barriers depending upon the constraint used to generate the twisted geometries.

3.1 The structural model used affects the retinal torsional properties

Because QM calculations of the retinal molecule are computationally demanding, simplified models have been used to derive its ground-state geometrical properties (e.g., [12, 35]). One simplification employed was to replace the C_9 and C_{13} methyl groups with hydrogen atoms. To assess how these simplifications affect the twisting properties of the retinal, we systematically assessed the torsional models for retinal models pSb1–pSb5 (Fig. 1) using constraint C-I.

The results summarized in Table 1 and Fig. 4 indicate that the absence of the methyl groups has a noticeable effect on the energy barriers for twisting the bonds in the $C_8 \cdots C_{15}$ segment. For example, the energy calculated for twisting the C_{12}–C_{13} and C_{13}=C_{14} bonds is approximately ~3–4 kcal/mol higher when computed with pSb2 than with pSb1. That is, the presence of the methyl groups on C_{13} makes the retinal less stable with respect to isomerization of the main-chain bonds involving C_{13}. The observation that the torsional barrier for the C_{13}=C_{14} bond is ~3 kcal/mol higher for pSb2 than for pSb1 (Table 1) is compatible with earlier modified neglect of diatomic overlap-correlated (MNDOC) calculations on C_{13}-substituted retinal analogs [11].

The absence of the β-ionone ring has a negligible effect on the torsional barriers in the Schiff base segment, but affects significantly the energy for twisting the C_6–C_7 bond: compared with pSb1 and pSb2 (Fig. 2a, b), this energy is ~6 kcal/mol higher in the case of models that do not contain the β-ionone ring (Fig. 2c–e). The noticeably higher torsional barrier of the C_6–C_7 bond in the absence of the β-ionone ring is largely due to the absence of the methyl group on C_5.

Absence of both the C_9/C_{13} methyl groups and of the β-ionone ring (pSb4 and pSb5, Fig. 2d, e) changes qualitatively the profile of the torsional energy barriers along the retinal chain (Fig. 4). Whereas in pSb2 it costs less energy to twist the C_{13}=C_{14} double bond than the adjacent C_{14}–C_{15}

Table 1 How the torsional barriers depend on the retinal model and the constraint used (see also Figs. 4, 5)

Retinal model	Energy barriers (kcal/mol) for twisting at 90° selected retinal bonds					
	C_6–C_7	C_8–C_9	C_{12}–C_{13}	C_{13}=C_{14}	C_{14}–C_{15}	C_{15}=N
Constraint C-I						
pSb1	4.6	14.8	23.0	20.9	26.3	17.8
pSb2	6.0	19.2	27.2	23.9	27.6	18.9
pSb3	10.3	12.2	20.8	22.6	25.3	19.7
pSb4	10.8	15.9	25.1	28.5[a]	26.1	20.9
pSb5	11.1	16.6	26.6	27.1	28.6	18.4
Constraint C-II						
pSb1	4.8	15.0	23.5	23.5	27.6	28.0
pSb5[b]	11.2	17.0	28.3	29.7	30.4	28.8

Constraints C-I and C-II are defined in Fig. 3

Except for a, all energy values reported here were computed at the B3LYP/6-31G* level using Gaussian98

[a] B3LYP/6-31G** value

[b] The C-II torsional values for pSb5 presented here reproduce those from Ref. [12] computed for the same retinal Schiff base model

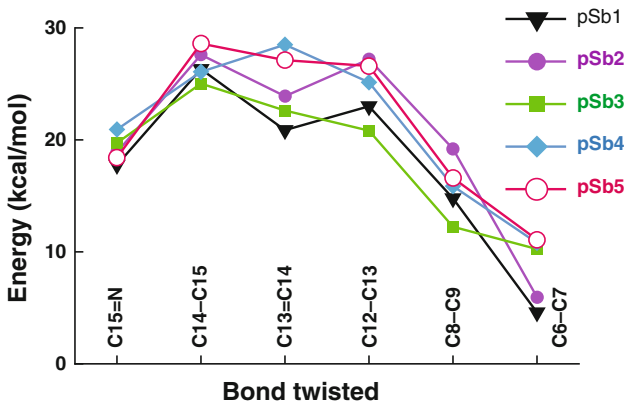

Fig. 4 How the torsional barrier depends on the retinal model. All torsional energy barriers (in kcal/mol) were computed with B3LYP/6-31G* using constraint C-I (see Table 1 for the exact values of the energy barriers, and Fig. 3a for the definition of the C-I constraint). The energy barriers for twisting around specific bonds of the retinal models pSb1, pSb2, pSb3, pSb4, and pSb5 are shown in *black triangles*, mauve *filled circles*, *green squares*, *cyan diamonds*, and *red empty circles*, respectively

and C_{12}–C_{13}, in pSb4 and pSb5 the three energy barriers are rather similar. For example, in pSb1 the energy for twisting the single-bonds C_{12}–C_{13} and C_{14}–C_{15} is, respectively, ~2 kcal/mol and ~5 kcal/mol higher than the energy for twisting C_{13}=C_{14}. In the case of pSb5, the energies for twisting C_{12}–C_{13} or C_{13}=C_{14} are noticeably higher than for pSb1, such that twisting C_{12}–C_{13} or C_{13}=C_{14} costs approximately the same energy (26.6 vs. 27.1 kcal/mol), which is also within 2 kcal/mol of the torsional barrier for the C_{14}–C_{15} bond (see Table 1; Fig. 4).

3.2 Effect of constraints on the retinal torsional barriers

Inspection of the 90°-twisted geometries generated using constraint C-I indicates that, for some of them, the C_i–R and C_{i-1}–R bonds (where R ≡ H or R ≡ C–H_3) is not in the same plane with the main-chain bonds of the C_i and C_{i-1} atoms that form the bond being twisted. We quantified the out-of-planarity geometries of the twisted pSb1 and pSb5 by calculating pyramidality dihedral angles for selected main-chain atoms (see Fig. 3d for the definition of the pyramidality dihedral angle). The pyramidality is largely restricted to the two atoms that form the bond being twisted and is larger toward the protonated Schiff base (Fig. 5).

The triple constraint C-II ensures that the C_i–R and C_{i-1}–R are coplanar with the main-chain bonds of the C_i and C_{i-1} atoms. As a result, the energy barriers for twisting around bonds involving atoms that experience noticeable pyramidalization with constraint C-I are larger when computed with C-II (Table 1). Consistent with the marked pyramidality of the nitrogen atom in both pSb1 and pSb5 computations (Fig. 5), there is a significant difference between the C-I and C-II torsional barriers (~10 kcal/mol) for the C_{15}=N. For the other bonds in the Schiff base segment, the increase in the torsional barrier when using C-II is within ~1.5–2.8 kcal/mol for both pSb1 and pSb5 and negligible for the C_6–C_7, C_8–C_9, and C_{12}–C_{13} bonds of pSb1 (Table 1).

To further assess the dependence of the torsional potentials on the constraint used to generate the 90°-twisted geometry, we performed a separate set of computations for the twist around C_{13}=C_{14} using constraint C-III (see Fig. 3d for the definition of the C-III constraint). The use of C-III ensures that at the 90° value of the constraint the pyramidalities of atoms C_{13} and C_{14} are close to zero (0.2° and 0.5°, respectively). The peak in the energy profile, 23.4 kcal/mol, is reached at a value of the C_{12}–C_{13}=C_{14}–C_{15} dihedral angle of 93° (Fig. 6a, b). This is almost identical with the energy barrier obtained with C-II.

Twisting at 90° of a specific bond may be accompanied by noticeable twists in the neighboring main-chain bonds

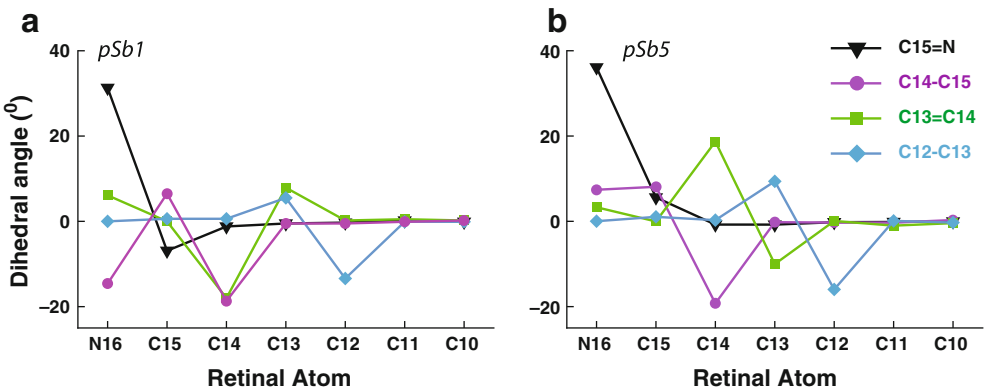

Fig. 5 Pyramidality of the retinal main-chain atoms upon bond twisting with constraint C-I in **a** pSb1 and **b** pSb5. See Fig. 3d for the definition of the pyramidality dihedral angle used here

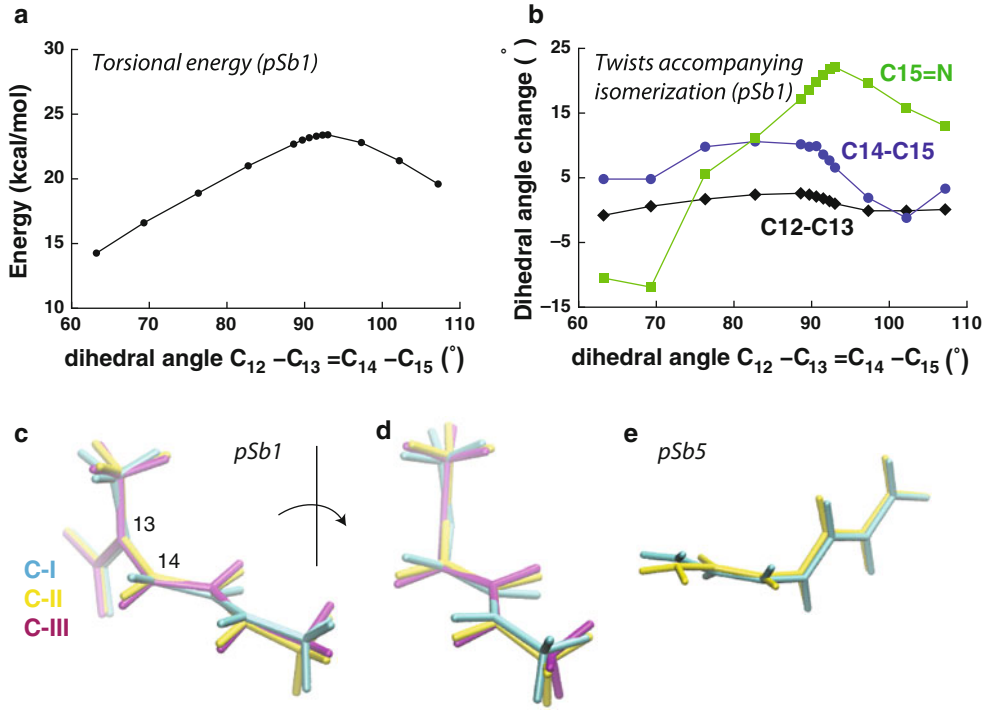

Fig. 6 Dependence of the torsional energy on the constraint used to rotate around the carbon–carbon bond. Illustration for the C_{12}–C_{13}=C_{14}–C_{15} dihedral angle of pSb1 using the C-III constraint (Fig. 3c). **a** The C-III torsional energy profile for the C_{13}=C_{14} bond for values of the C-III-constraint of 60°, 65°,…,80°, 81°, 82°, 83°, 84°, 85°, 90°, 95°, 100° (see Fig. 3c for the definition of the C-III constraint). The energy profile (energies in kcal/mol, B3LYP/6-31G* values) is represented as a function of the C_{12}–C_{13}=C_{14}–C_{15} dihedral (degrees) as measured for each value of C-III. The C-III torsional profile was computed using the Gaussian03 package [107]. Compare Fig. 6a to Table 1 and Figs. 4 and 7a. **b** Changes in dihedral angles of the Schiff base segment along the C-III path for the C_{13}=C_{14} bond. The change in each of the dihedral angles (reported in degrees) was taken relative to 180°. Note the *marked changes* in the C_{14}–C_{15}=N–Cε dihedral angle. **c**–**d** Comparison of the twisted geometries of pSb1 at the 90° value of constraints C-I (*cyan*), C-II (*yellow*) and C-III (*purple*). For simplicity, in the images, retinal is truncated at C_{12} in **d**, and at C_{13} in **d**. We note that at a value of 0° of the C-III constraint the retinal is 13,14-*dicis*, with values of the C_{12}–C_{13}=C_{14}–C_{15}, C_{13}=C_{14}–C_{15}=N, and C_{14}–C_{15}=N–Cε of −1.3°, −8.9°, and 179.7°, respectively; at a 50 value of the C-III constraint for the C_{13}=C_{14} twist, retinal is 13-*cis*, with values of the C_{12}–C_{13}=C_{14}–C_{15}, C_{13}=C_{14}–C_{15}=N, and C_{14}–C_{15}=N–Cε of 5.0°, −179.7, and −178.7°, respectively. **e** Comparison of the twisted geometries of pSb5 at the 90° value of constraints C-I (*cyan*) and C-II (*yellow*), showing retinal truncated at C_9

(Fig. 6b–d). For example, C-III twisting of the C_{13}=C_{14} bond is accompanied by twisting with up to ∼22° of the C_{15}=N bond (Fig. 6b).

To assess systematically the change in the retinal geometry that accompanies twisting of specific bonds in pSb1, we fully optimized the *trans–cis* isomerization paths of pSb1 in the gas phase using the CPR algorithm [75] and SCC-DFTB [72] to describe the retinal chromophore. It has been shown that relative to full DFT, the SCC-DFTB method gives a reasonable description of the torsional properties of the retinal not only in the gas phase [90], but also in the protein environment [77].

The results summarized in Figs. 7 and 8 indicate that the isomerization around the C_{13}=C_{14} or C_{15}=N double bonds is accompanied by significant changes in the twisting of C_{15}=N and C_{13}=C_{14}, respectively (Figs. 7c, k, 8). Isomerization around C_{14}–C_{15} is accompanied by minor changes of the C_{15}=N and C_{13}=C_{14} twists and a somewhat larger twisting of C_{12}–C_{13} (Fig. 7g, 8).

3.3 Effect of a hydrogen-bonding water molecule on the torsional properties of the Schiff base segment

The torsional barrier may depend on whether or not the Schiff base hydrogen bonds to water. We performed preliminary test computations on pSb1 in the presence of a water molecule that hydrogen bonds to the Schiff base (i.e., corresponding to w402 in Fig. 1a); for these tests, we employed constraints C-I or C-II and B3LYP/6-31G*. The presence of the water molecule slightly increases the bond alternation of the retinal Schiff base: Compared to pSb1 in the absence of water and in the presence of the water molecule, the C_{15}=N and C_{13}=C_{14} bonds are 0.007 Å shorter, and the C_{14}–C_{15} and C_{12}–C_{13} bonds are longer, respectively, by 0.008 and 0.007 Å. The more pronounced bond alternation would mean that the torsional barriers for the double bonds should increase, whereas those for the single bonds should decrease. Indeed, this is what we

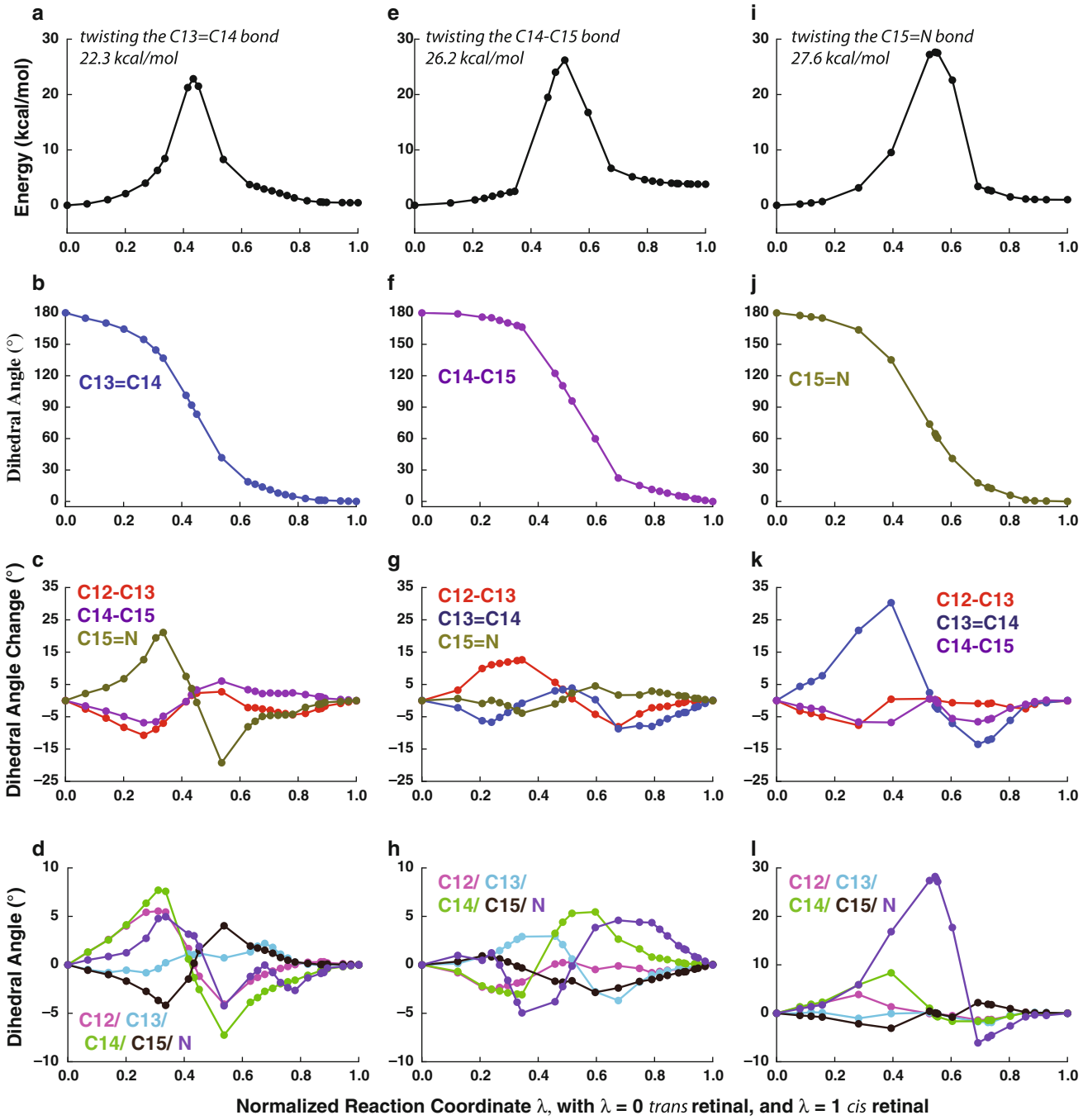

Fig. 7 Pathways for twisting retinal bonds in the Schiff base segment. The twisting of the retinal C_{13}=C_{14} (**a**–**d**), C_{14}–C_{15} (**e**–**h**), and C_{15}=N (**i**–**l**) were computed with CPR [75] using SCC-DFTB [72] to describe the retinal. The retinal model used in these computations is depicted in Figs. 2a and 6a. For each of the pathway, we show the energy profile (**a**, **e, i**), the change of the dihedral angle describing the bond being isomerized (**b**, **f, j**), the variation of the nearby dihedral angles, taken relative to the reference value of 180° in the planar all-*trans* retinal (**c**, **g**, **k**), and the pyramidality of selected carbon atoms in the Schiff base segment (**d**, **h**, **l**). Energy values are given in kcal/mol, and dihedral angles are given in degrees. All *plots* are represented as a function of the normalized reaction coordinate λ, which is the sum along the path of the change in all atomic coordinates computed as a root-mean-squared difference [75]. For all paths, retinal is all-*trans* at $\lambda = 0$ and *cis* at $\lambda = 1$. See Fig. 8 for geometries of the retinal at selected points along the paths

observe. Relative to the calculations in the absence of a water molecule (Table 1), the C-I torsional energy barriers for the single-bond C_{12}–C_{13} and C_{14}–C_{15} are lower by 3.9 and 1.6 kcal/mol, whereas the C_{13}=C_{14} and C_{15}=N torsions are higher by 4.3 and 3.1 kcal/mol, respectively. The trend is confirmed by test calculations using the C-II constraint.

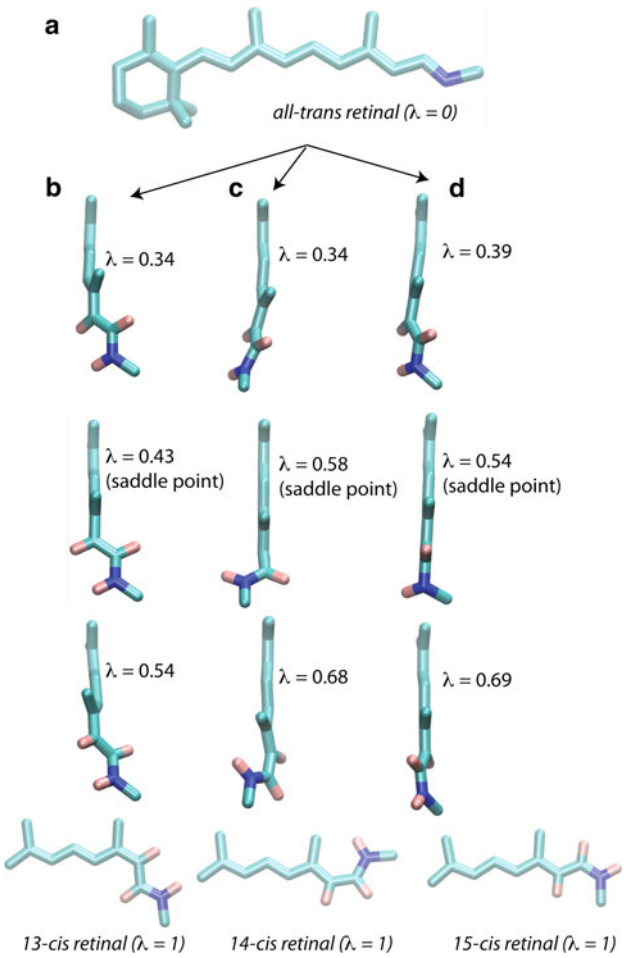

Fig. 8 The geometry of the retinal in the isomerization paths computed with CPR and SCC-DFTB. All paths started from all-*trans* retinal (**a**). For each of the paths depicted in Fig. 7, we show the final *cis* geometry, and three intermediate points along the path. The three intermediate points for each path are the saddle point, and two points on either side of the saddle point that correspond to values of extreme variations of dihedral angles other than that describing the isomerized bond. For example, in set (**b**) of the panels for isomerizing the C_{13}=C_{14} bond, the geometries at $\lambda = 0.34$ and $\lambda = 0.54$ correspond to the largest positive and, respectively, largest negative twist of the C_{15}=N bond that accompanies the isomerization of the C_{13}=C_{14} bond (see Fig. 7c). For simplicity, only selected retinal atoms are shown in **b**–**d**. Carbons atoms are shown in *cyan*, nitrogen—*blue*, and hydrogen atoms—*pink*

With C-II, the torsional barriers for C_{12}–C_{13} and C_{14}–C_{15} are 3.4 kcal/mol and 3.2 kcal/mol, respectively, lower in the presence than in the absence of the hydrogen-bonding water molecule; the C_{13}=C_{14} bond twist is 4.1 kcal/mol more costly in the presence than in the absence of the water molecule.

We note that in addition to the effect on the bond alternation in the all-*trans* geometry, the presence of the water molecule hydrogen-bonding to the retinal Schiff base can also influence the change in the retinal bond alternation in the 90°-twisted geometries relative to all-*trans*, and some of the changes in retinal geometry that accompany the bond twists. We monitored the change in the retinal bond lengths (relative to the all-*trans* geometry) when the C_{13}=C_{14} and C_{14}–C_{15} bonds are twisted to 90°: It has been shown before that at a C–C single-bond 90° twist, the positive charge is largely localized in the Schiff base segment, that is, the conjugation in the Schiff base segment of the twisted structure is much smaller than in all-*trans*; the bond alternation toward the C_6 end of the polyene chain is significantly larger (i.e., longer single bonds, shorter double bonds) than in the all-*trans* conformer. For C=C double-bond 90° twists, the single bonds become shorter than in all-*trans*, the double bonds become longer, and the positive charge is transferred away from the Schiff base, with the Schiff base segment being converted into a neutral enamine (see Ref. [12] for detailed discussions). We find here that the change in the retinal bond lengths upon twisting at 90°, the C_{13}=C_{14} bond is almost identical in the presence and in the absence of a water molecule hydrogen-bonding to the retinal Schiff base. In the case of the C_{14}–C_{15} 90° twist, however, the bond alternation in the Schiff base segment increases somewhat more when the water molecule is present (by up to 0.01 Å in the case of the C_{14}–C_{15} bond). In the presence of the water, the pyramidalization at the N_{16} atom observed when twisting the C_{14}–C_{15} or C_{13}=C_{14} bonds (Fig. 5a) is reduced to $\sim$3° and $\sim$0° when the water molecule is present; a reduced pyramidalization at N_{16} is not observed for the C_{15}=N twist.

3.4 Torsional barriers calculated with recent DFT functionals

Inspection of the bond lengths of pSb1 optimized with different DFT functionals (Fig. 9a, b) indicates subtle differences between the bond alternation in the Schiff base segment with B3LYP as compared to BMK, CAM-B3LYP, M05-2X, and M06-2X. Whereas with B3LYP, the C_{13}=C_{14} and C_{12}–C_{13} bonds have almost identical lengths (within 0.003 Å), with the latter three functionals C_{12}–C_{13} is slightly longer than C_{13}=C_{14} (e.g., by 0.01 Å with BMK). LC-wPBE gives a pronounced bond alternation (Fig. 9b) that resemble results from HF calculations [42]. The pattern of the dihedral angle torsional energy barriers (Fig. 9c) is consistent with the bond alternation; whereas with B3LYP and B3PW91 it costs $\sim$5 kcal/mol less energy to twist C_{13}=C_{14} than C_{14}–C_{15}, with BMK, for example, twisting C_{13}=C_{14} is 1.7 kcal/mol energetically more expensive than twisting C_{14}–C_{15}.

4 Conclusion

Several different force fields for the retinal chain have been developed and used in MM computations of retinal

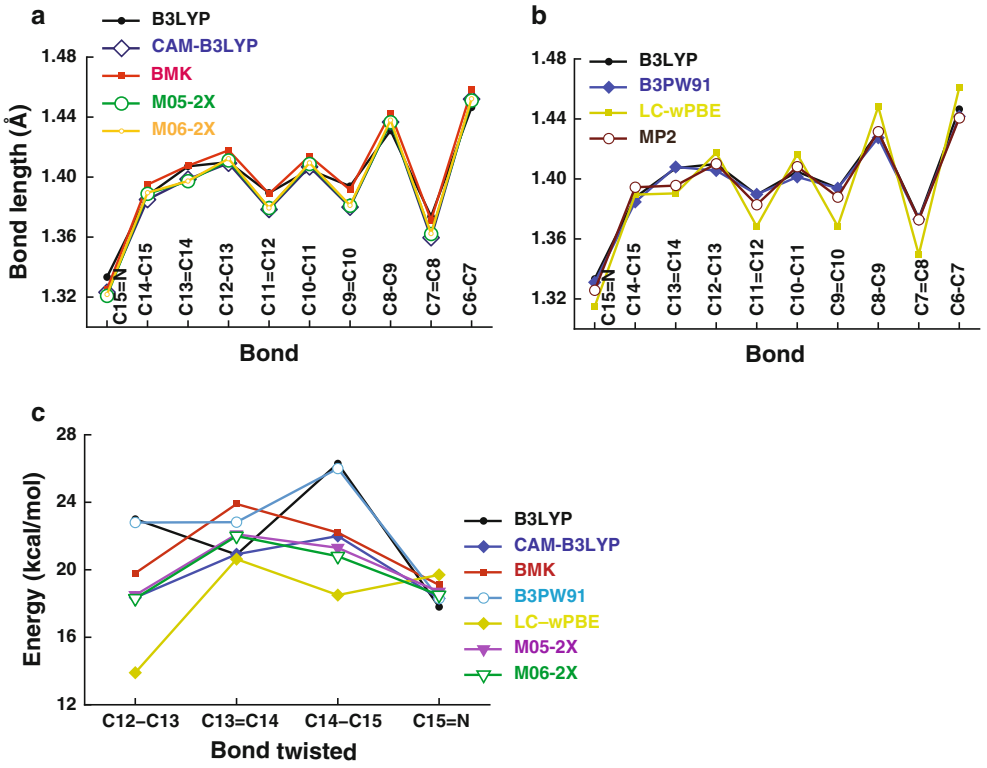

Fig. 9 Retinal bond alternation and torsional barriers calculated with different DFT functionals. All calculations were performed with a 6-31G* basis set and model pSb1. **a**, **b** Retinal bond alternation. The bond lengths are reported in Å. Note that with B3LYP, the C_{13}=C_{14} bond is slightly longer than the adjacent C_{14}–C_{15} and has almost the same length as C_{12}–C_{13} (the C_{12}–C_{13}, C_{13}=C_{14}, and C_{14}–C_{15} bond lengths are 1.41, 1.407, and 1.39 Å, respectively). The same trend is observed for B3PW91. With BMK, M05-2X, and M06-2X, the C_{12}–C_{13} bond is slightly longer than C_{13}=C_{14} (1.42 Å vs. 1.41 Å in the case of BMK). LC-wPBE values are very close to MP2 for the Schiff base segment, but give a large bond alternation for the remaining segment of the retinal. **c**. Energy barriers (in kcal/mol) for twisting retinal at 90° using constraint C-I. Note that the B3LYP and B3PW91 barriers follow the same trend. M05-2X and M06-2X give very similar values

proteins. The force fields may be distinguished for example, by the QM method used, the retinal Schiff base model used, or by whether or not interactions with water molecules or other parts of the protein environment are taken into consideration for deriving the atomic partial charges. The torsional parameters used for the retinal polyene chain bonds will largely determine retinal's flexibility and preferred conformation, whereas the partial charges of retinal atoms that in the protein environment can hydrogen bond to protein groups or to water molecules (Fig. 1) will influence significantly the strength of these hydrogen bonds.

By computing the torsional energy barriers for five different retinal protonated Schiff base models (Fig. 2), we quantified the influence of the retinal model used on the torsional potential at the B3LYP/6-31G* level (Table 1; Fig. 4). Both the β-ionone ring and the methyl groups on the C_9 and C_{13} atoms lower the energy barrier for twisting the nearby bonds. That is, the energy barriers for twisting the C_{12}–C_{13} and C_{13}=C_{14} are noticeably smaller in pSb1 (Fig. 2a) than in retinal models that lack the C_9 and C_{13} methyl groups (Fig. 2b, d, e). Likewise, twisting the C_6–C_7 bond costs significantly less energy in pSb1 than in models lacking the β-ionone ring. As a consequence, a MM computation based on retinal torsional parameters derived from a simplified model without the C_9 and C_{13} methyl groups and without the β-ionone ring will render a retinal molecule more rigid than if it were described with parameters from the complete retinal molecule, pSb1. Due to the close interactions between retinal and its protein environment (Fig. 1), the geometry and the flexibility of the retinal could affect the structure and dynamics of the protein. A strong coupling between retinal and the protein was indeed demonstrated, for example, by prolonged molecular dynamics simulations on squid rhodopsin [36], observations of a significant effect of the protein environment close to the β-ionone ring on the induced dipole moment of the retinal in bacteriorhodopsin [91], and experiments indicating that modifications of the β-ionone ring affect the photocycle of sensory rhodopsin I [92].

An additional complication in comparing the torsional potentials of the retinal arises from the need to account for

pyramidalization, in particular in the case of twisting bonds of the Schiff base segment (Figs. 5, 7d, h, l), and twisting of bonds other than that being isomerized may also accompany isomerization in the both pSb1 and pSb5 models tested (Figs. 6c–e, 7c, g, k). We find that twisting of the C_{13}=C_{14} bond is very sensitive to isomerization around C_{15}=N and, likewise, the C_{14}–C_{15}=N–Cε dihedral angle is very sensitive to the isomerization of the C_{13}=C_{14} bond (Figs. 6b–e, 7c, k). As a consequence of the geometry changes that accompany bond twisting, the torsional parameters for the Schiff base segment may depend on the constraint used (see Table 1; Figs. 6, 7).

The importance of polarization effects for retinal proteins was demonstrated by Warshel and co-workers, who also account for polarization in their works by using QCFF/PI and coupling to the electrostatic environment (see, for example, Refs. [22–24, 28, 54]). A recent survey [59] of MM MD papers on bacteriorhodopsin performed with the CHARMM, GROMACS, or AMBER force fields highlighted what appear to be systematic deficiencies of some of the MM treatments of the retinal-binding pocket, at least in the case of bacteriorhodopsin. For example, it was noted that the crystal-structure arrangement in which the Schiff base hydrogen bonds to w402 (Fig. 1a) is lost in the MM simulations from Refs. [93] and [94]. In Ref. [95], it was also noted that within a MM description the water molecules close to the retinal Schiff base are very mobile and attributed the formation of the Schiff base–Asp85 direct interaction to the lack of polarization [95, 96].

To assess whether lack of polarization could account for the difficulties in maintaining the crystal-structure geometry in MM MD simulations, in Ref. [59] a polarized force field was derived by re-optimizing with DFT/MM the partial charges of the protonated retinal and 23 amino acids of the retinal-binding pocket. The use of the re-optimized MM charges led to the structure of the bacteriorhodopsin retinal-binding pocket being stable during MD [59]. Since the MD simulations in Ref. [59] were performed without explicit treatment of the lipid membrane, and by constraining to the crystal-structure coordinates of the Cα atoms of significant portions of the cytoplasmic and extracellular parts of the protein, it would be interesting to see how the DFT/MM re-optimized charges would perform for a fully flexible bacteriorhodopsin trimer embedded in a hydrated lipid membrane. Another potentially valuable improvement to the description of the retinal proteins within the context of CHARMM would be to add coupling terms to describe the structural changes of the retinal chain that accompany the bond twists identified here. For example, significant improvement in describing the energies and energy derivatives of distorted structures was obtained when using a force field that accounts for bond and angle anharmonicity, and cross-term interactions between bond stretch and valence angle bending, bonds stretch and dihedral angle torsion, and between angle bending and torsion [97, 98].

The derivation of parameters for the neutral retinal Schiff base, which poses the additional challenge of describing the isomerization of true double bonds, may benefit from the recent developments in the molecular orbital description of bi-radical species [99]. Likewise, test computations [100, 101] suggest that recent DFT functionals could improve the description of the proton transfer energetics and of the hydrogen-bonded networks in the active site of retinal proteins. We report here that preliminary test computations (Fig. 9) would suggest the recent DFT functionals BMK, M05-2X, or M06-2X, as potentially suitable for exploring the potential energy surface of the protonated retinal molecule: when using either of these three functionals, the torsional barrier for twisting around the C_{13}=C_{14} bond is no longer smaller than the barriers for C_{12}–C_{13} and C_{14}–C_{15} (Fig. 9c). That is, the BMK, M05-2X, and M06-2X functionals appear to correct for the overpolarization of the protonated retinal molecule indicated by B3LYP and B3PW91 (Fig. 9). In the future, it would be of interest to further assess the applicability of the recent DFT functionals to retinal proteins reactions by performing detailed benchmark computations of proton transfer reactions, for example.

The quality of the force-field parameters for the retinal molecule is ultimately assessed by comparison with experimental data such as crystal-structure geometry, or the rate-limiting barriers for retinal thermal isomerization. A strict validation of all parameters required for the force field may be rendered nontrivial by the inherent difficulty in accurately solving the atomic coordinates of the twisted retinal molecule interacting with a complex counterion [29]. Indeed, it has been noted that crystal structures of bacteriorhodopsin intermediate states do not capture the effect of protonation and of the counterion interaction on the retinal bond alternation [42], and details of the retinal geometry incompatible with the presumed reaction path have been identified in experiments [102] and theory [18, 103].

Acknowledgments This work has been supported in part by the Deutsche Krebsforschungszentrum and by the Deutsche Forschungsgemeinschaft (SM 63/7). J. C. S. was supported by a Laboratory-Directed Research and Development grant from the United States Department of Energy. A.-N. B. was supported in part by grants GM74637 and GM086685 from the National Institutes of General Medical Sciences (at UC Irvine) and by a Marie Curie International Reintegration Grant (FP7-PEOPLE-2010-RG 276920) at the Freie Universität Berlin. We thank the Norddeutscher Verbund für Hoch- und Höchstleistungsrechner (HLRN) for an Award of computing time (to A.-N. B).

References

1. Herzfeld J, Lansing JC (2002) Annu Rev Biophys Biomol Struct 31:73
2. Hirai T, Subramaniam S (2003) FEBS Lett 545:2
3. Lanyi JK (2004) Annu Rev Physiol 66:665
4. Neutze R, Pebay-Peyroula E, Edman K, Royant A, Navarro J, Landau EM (2002) Biochim Biophys Acta 1565:144
5. Wise KJ, Gilespie NB, Stuart JA, Krebs MP, Birge RR (2002) Trends Biotech 20:387
6. Adamantidis AR, Zhang F, Aravanis AM, Deisseroth K, de Lecea L (2007) Nature 450:420
7. Zhang F, Wang L-P, Brauner M, Liewald JF, Kay K, Watzke N, Wood PG, Bamberg E, Nagel G, Gottschalk A, Deisseroth K (2007) Nature 446:633
8. Kleinlogel S, Feldbauer K, Dempski RE, Fotis H, Wood PG, Baman C, Bamberg E (2011) Nature Neurosci 14:513
9. Tye KM, Prakash R, Kim S-Y, Fenno LE, Grosenick L, Zarabi H, Thompson KR, Gradinaru V, Ramakrishnan C, Deisseroth K (2011) Nature 471:358
10. Garavelli M, Vreven T, Celani P, Bernardi F, Robb MA, Olivucci M (1998) J Am Chem Soc 120:1285
11. Tavan P, Schulten K, Gärtner W, Oesterhelt D (1985) Biophys J 47:349
12. Tajkhorshid E, Paizs B, Suhai S (1999) J Phys Chem B 103:4518
13. Wanko M, Hoffmann M, Strodel P, Koslowski A, Thiel W, Neese F, Frauenheim T, Elstner M (2005) J Phys Chem B 109:3606
14. Weingart O, Schapiro I, Buss V (2007) J Phys Chem B 111:3782
15. Altun A, Yokoyama S, Morokuma K (2008) J Phys Chem B 112:16883
16. Murata K, Fujii Y, Enomoto N, Hata M, Hoshino T, Tsuda M (2000) Biophys J 79:982
17. Baudry J, Crouzy S, Roux B, Smith JC (1999) Biophys J 76:1909
18. Bondar A-N, Baudry J, Suhai S, Fischer S, Smith JC (2008) J Phys Chem B 112:14729
19. Sugihara M, Buss V, Entel P, Elstner M, Frauenheim T (2002) Biochemistry 41:15259
20. Tajkhorshid E, Suhai S (1999) Chem Phys Lett 299:457
21. Tavan P, Schulten K, Oesterhelt D (1985) Biophys J 47:415
22. Warshel A (1978) Proc Natl Acad Sci USA 75:2558
23. Warshel A, Deakyne C (1978) Chem Phys Lett 55:459
24. Warshel A (1979) Photochem Photobiol Sci 30:291
25. Warshel A, Barboy N (1982) J Am Chem Soc 104:1469
26. Singh UC, Kollman P (1986) J Comp Chem 7:718
27. Field MJ, Bash PA, Karplus M (1990) J Comp Chem 11:700
28. Warshel A (1991) Computer modeling of chemical reactions in enzymes and solutions. John Wiley & Sons, New York
29. Okada T, Sugihara M, Bondar A-N, Elstner M, Entel P, Buss V (2004) J Mol Biol 342:571
30. Hayashi S, Tajkhorshid E, Kandori H, Schulten K (2004) J Am Chem Soc 126:10516
31. Bondar A-N, Fischer S, Suhai S, Smith JC (2005) J Phys Chem B 109:14786
32. Sugihara M, Fujibuchi W, Suwa M (2011) J Phys Chem B 115:6172
33. Murakami M, Kouyama T (2008) Nature 453:363
34. Brown MF (1994) Chem Phys Lipids 73:159
35. Nina M, Roux B, Smith JC (1995) Biophys J 68:25
36. Jardón-Valadez E, Bondar A-N, Tobias D (2010) Biophys J 99:2200
37. Tergesten F, Buss V (1996) J Mol Struct (Theochem) 369:53
38. Hamanaka T, Mitsui T, Ashida T, Kakudo M (1972) Acta Cryst B28:214
39. Champagne B, Perpète EA, Jacquemin D, van Gisbergen SJA, Baerends E-J, Soubra-Ghaoui C, Robins KA, Kirtman B (2000) J Phys Chem A 104:4755
40. Buda F, Giannozzi P, Mauri F (2000) J Phys Chem B 104:9048
41. Hufen J, Sugihara M, Buss V (2004) J Phys Chem B 108:20419
42. Bondar A-N, Smith JC, Elstner M (2010) Theor Chem Acc 125:353
43. Paizs B, Tajkhorshid E, Suhai S (1999) J Phys Chem B 103:5388
44. Tergesten F, Buss V (1998) J Mol Struct (Theochem) 430:209
45. Nina M, Smith JC, Roux B (1993) J Mol Struct (Theochem) 286:231
46. Brooks BR, Bruccoleri RE, Olafson BD, States DJ, Swaminathan S, Karplus M (1983) J Comput Chem 4:187
47. Ponder JW, Case DA (2003) Adv Prot Chem 66:27
48. Jorgensen WL, Tirado-Rives J (1988) J Am Chem Soc 110:1657
49. Oostenbrink C, Villa A, Mark AE, van Gunsteren WF (2004) J Comp Chem 25:1656
50. Hwang MJ, Stockfisch TP, Hagler AT (1994) J Am Chem Soc 116:2515
51. Warshel A (1977) Comput & Chem 1:195
52. Warshel A (1976) Nature 260:679
53. Warshel A, Chu YT (2001) J Phys Chem 105:9857
54. Warshel A, Chu ZT, Hwang J-K (1991) Chem Phys 158:303
55. Braun-Sand S, Sharma PK, Chu ZT, Pisliakov AV, Warshel A (2008) Biochem Biophys Acta 1777:441
56. Tajkhorshid E, Baudry J, Schulten K, Suhai S (2000) Biophys J 78:683
57. Baudry J, Tajkhorshid E, Molnar F, Phillips J, Schulten K (2001) J Phys Chem B 105:905
58. Friedman R, Nachliel E, Gutman H (2003) Biophys J 85:886
59. Babitzki G, Denschlag R, Tavan P (2009) J Phys Chem B 113:10483
60. MacKerell AD Jr (2004) J Comp Chem 25:1584
61. MacKerell AD Jr, Feig M, Brooks CL III (2004) J Comp Chem 25:1400
62. Baudry J, Crouzy S, Roux B, Smith JC (1997) J Chem Inf Comput Sci 37:1018
63. Nina M, Roux B, Smith JC (1992) Struct Funct Retinal Prot 221:17
64. Said M, Maynau D, Malrieu J-P, Garcia Bach M-A (1984) J Am Chem Soc 106:571
65. Roux B, Nina M, Pomès R, Smith JC (1996) Biophys J 71:670
66. Belrhali H, Nollert P, Royant A, Menzel C, Rosenbusch JP, Landau EM, Pebay-Peyroula E (1999) Structure 7:909
67. Luecke H, Schobert B, Richter H-T, Cartailler J-P, Lanyi JK (1999) Science 286:255
68. Hayashi S, Tajkhorshid E, Pebay-Peyroula E, Royant A, Landau EM, Navarro J, Schulten K (2001) J Phys Chem B 105:10124
69. Saam J, Tajkhorshid E, Hayashi S, Schulten K (2002) Biophys J 83:3097
70. Gruia AD, Bondar A-N, Smith JC, Fischer S (2005) Structure 13:617
71. Lemaître V, Yeagle P, Watts A (2005) Biochemistry 44:12667
72. Elstner M, Porezag D, Jungnickel G, Elner J, Haugk M, Frauenheim T, Suhai S, Seifert G (1998) Phys Rev B 58:7260
73. Matthies RA, Lugtenburg J (2000) Handbook of biological physics. Elsevier, Amsterdam, p 50
74. Frisch MJ et al (1998) GAUSSIAN 1998. Gaussian, Inc., Pittsburgh
75. Fischer S, Karplus M (1992) Chem Phys Lett 194:252
76. Cui Q, Elstner M, Kaxiras E, Frauenheim T, Karplus M (2001) J Phys Chem B 105:569

77. Bondar A-N, Suhai S, Fischer S, Smith JC, Elstner M (2007) J Struct Biol 157:454
78. Choi C, Elber R (1991) J Chem Phys 94:751
79. Yanai T, Tew DP, Handy NC (2004) Chem Phys Lett 393:51
80. Perdew JP (1986) Phys Rev B 33:8822
81. Perdew JP (1991) Electronic structure of solids. Akademie Verlag, Berlin, p 11
82. Becke AD (1992) J Chem Phys 97:9173
83. Perdew JP, Chevary JA, Vosko SH, Jackson KA, Pederson MR, Singh DJ, Fiolhais C (1992) Phys Rev B 46:6671
84. Perdew JP, Wang Y (1992) Phys Rev B 45:13244
85. Boese AD, Martin ML (2004) J Chem Phys 121:3405
86. Tawada Y, Tsuneda T, Yanagisawa S, Yanai T, Hirao K (2004) J Chem Phys 120:8425
87. Zhao Y, Schultz NE, Truhlar DG (2006) J Chem Theor Comput 2:364
88. Zhao Y, Truhlar DG (2008) Theor Chem Acc 120:215
89. Frisch MJ et al (2009) Gaussian 09. Gaussian, Inc., Wallingford
90. Zhou H, Tajkhorshid E, Frauenheim T, Suhai S, Elstner M (2002) Chem Phys Lett 277:91
91. Aharoni A, Khatchatouriants A, Manevitch A, Lewis A, Sheves M (2003) J Phys Chem B 107:6221
92. Yan B, Takahashi T, McCain DA, Rao VJ, Nakanichi K (1990) Biophys J 57:477
93. Kandt C, Schlitter J, Gerwert K (2004) Biophys J 86:705
94. Grudinin S, Bueldt G, Gordeliy V, Baumgaertner A (2005) Biophys J 88:3252
95. Baer M, Mathias G, Kuo I-F W, Tobias DJ, Mundy CJ, Marx D (2008) ChemPhysChem 9:2703
96. Chaumont A, Baer A, Mathias G, Marx D (2008) ChemPhysChem 9:2751
97. Maple JR, Hwang M-J, Stockfisch TP, Dinur U, Waldman M, Ewig CS, Hagler AT (1994) J Comp Chem 15:162
98. Maple JR, Hwang M-J, Jalkanen KJ, Stockfisch TP, Hagler AT (1998) J Comp Chem 19:430
99. Saito T, Nishihara S, Yamanaka S, Kitagawa Y, Kawakami T, Yamada S, Isobe H, Okumura M, Yamaguchi K (2011) Theor Chem Acc. doi:10.1007/s00214-0941-9
100. Song J-W, Tsuneda T, Sato T, Hirao K (2011) Theor Chem Acc. doi:10.1007/s00214-011-0997-6
101. Yamabe S, Kawagishi N (2011) Theor Chem Acc. doi:10.1007/s00214-011-0929-5
102. Bajaj VS, Mak-Jurkauskas ML, Belenky M, Herzfeld J, Griffin RG (2009) Proc Natl Acad Sci USA 106:9244
103. Bondar A-N, Smith JC, Fischer S (2006) Photochem Photobiol Sci 5:547
104. Humphrey W, Dalke AK, Schulten K (1996) J Mol Graph 14.1:33
105. Schobert B, Cupp-Vickery J, Hornak V, Smith SO, Lanyi JK (2002) J Mol Biol 321:715
106. Nakamishi H, Okada T (2006) Angew Chem Int Ed 45:4270
107. Frisch MJ et al (2004) Gaussian 03. Gaussian, Inc., Wallingford